IEEE Access
Multidisciplinary ⋮ Rapid Review ⋮ Open Access Journal

Received 19 July 2023, accepted 16 August 2023, date of publication 28 August 2023, date of current version 15 September 2023.

Digital Object Identifier 10.1109/ACCESS.2023.3309553

RESEARCH ARTICLE

Sparse Inversion of Aerosol Concentration Distribution Based on LIDAR Remote Sensing

WEIYI WANG[1,2], DONGSHENG YU[2], HAIBO YU[2,1], MINGHAN YANG[2], CHIDONG XU[2], AND XIAODONG FANG[2]

[1]Science Island Branch, Graduate School, University of Science and Technology of China, Hefei, Anhui 230026, China
[2]Hefei Institutes of Physical Science, Chinese Academy of Sciences, Hefei, Anhui 230031, China

Corresponding author: Chidong Xu (xcd@aiofm.ac.cn)

This work was supported by the Civil Space Program under Grant D010206.

ABSTRACT Measuring the distribution of atmospheric aerosol concentration is of great significance for accurately assessing the scale of explosions and fires, the evolution of atmospheric environment, and so on. Due to the effect of atmospheric diffusion and other complex meteorological conditions, the distribution of aerosol concentration will change significantly in a short period of time, which puts higher requirements on the speed of aerosol concentration measurement. The existing measurement technology mainly uses LIDAR for intensive sampling of aerosol in a region. Although lidar can achieve accurate measurement of the average concentration of atmospheric aerosol more conveniently, due to longer data processing time and more measurement sampling times, the timeliness of lidar remote sensing has decreased, resulting in the problem of difficult to capture the shape of atmospheric smoke and clouds in a timely manner. Therefore, this study proposes a fast reconstruction deep network model of aerosol extinction coefficient for lidar remote sensing from the perspective of sparse sampling-reconstruction. This model eliminates the feature distribution difference between lidar return signals under sparse sampling and conventional dense sampling by using unsupervised generative adversarial networks from the perspective of transfer learning. Then, the extinction coefficient reconstruction network with the encoding-decoding structure maps the low-dimensional abstract features of aerosol concentration distribution back to the high-dimensional extinction coefficient representation space. This model greatly reduces the sampling number of lidar, thereby reducing the total time required for aerosol extinction coefficient inversion. Experimental measurements of smoke and clouds above a thermal power plant show that the proposed deep network model can reduce more than 50% of the lidar sampling times within the allowable error range. This indicates that the model has the ability to significantly improve the remote sensing measurement efficiency of lidar for atmospheric aerosols.

INDEX TERMS LIDAR, aerosol extinction coefficient, deep learning, inverse problem, fast reconstruction.

I. INTRODUCTION

Aerosols are the dominant uncertainty in assessing anthropogenic forcing of climate change. Their distribution in space and time domain are highly asymmetrical and variable. Meanwhile, aerosols have an important impact on global climate change, atmospheric environment quality, ecological balance, human health. It also has important scientific significance and application value in many fields such as weather forecast, military observation, atmospheric light transmission and remote sensing application [1], [2], [3]. Therefore, accurate measurements of the distribution of aerosol properties are important for understanding climate change [4], [5].

Previously, aerosol concentration was measured by offline sampling, which has a low efficiency, and is difficult to accurately measure the concentration distribution. With the development of optical remote sensing technology, especially active remote sensing, LIDAR [6] has gradually become one of the important methods for aerosol concentration measurement. At present, the development of hardware and algorithm of LIDAR is gradually maturing. A variety of LIDAR types, including Mie scattering lidar [7], [8], [9], polarized lidar,

The associate editor coordinating the review of this manuscript and approving it for publication was Cheng Hu.

Raman lidar, high spectral resolution lidar, fluorescent lidar, etc, have been built and widely used. Due to the obvious influence of various natural factors and human activities on the atmosphere, especially the lower boundary layer in the atmosphere, the aerosol detection requirements become more and more complex, which brings great challenges to the LIDAR data processing algorithm. As we know, the key problem of aerosol concentration reconstruction is extinction coefficient inversion. For the extinction coefficient inversion, Collis slope method [7], [10], Klett stable analytical method [11] and Fernald integral method [12], [13] were proposed successively, and Fernald integral has become the current mainstream method. On this basis, least square, Newton and Secant methods were introduced to solve the extinction coefficient boundary and backscatter ratio, which are key parameters in Fernald integral method.

At present, in addition to the above LIDAR algorithm research, a problem to be solved is how to reconstruct the exact extinction coefficient [14] based on sparse scanning sampling, and then obtain the aerosol concentration distribution, which has great significance for atmospheric detection, that is, we can reconstruct aerosol concentration based on LIDAR remote sensing more quickly, and improve the timeliness of detection. However, under the existing framework, the feasible reconstruction method is based on the sparse concentration distribution retrieved by the Fernald integral, Klett, Collis slope or other methods, and the complete concentration distribution is reconstructed by interpolation methods such as nearest neighbor and bilinear. Although this can meet the timeliness requirements of reconstruction, it greatly reduces the reconstruction accuracy. The problems with the previous methods focused on two main aspects. Firstly, the method simplifies the actual inversion formula by putting forward some assumptions. For example, the Collis slope method assumes that the extinction coefficient and backscattering sparsity are constant values at the same height. Since some hypothetical information is added artificially, the accuracy of the algorithm is greatly affected. In other words, the previous methods only invert the approximate extinction coefficient. Secondly, even if the principle formula is simplified, the time complexity of the algorithm is still very high which makes the real-time reconstruction of extinction coefficient difficult to achieve.

With the development of artificial intelligence, machine learning, especially deep learning, provide additional solutions to inverse problems, for example, signal compression and recovery, computer tomography, particle energy spectrum solution, et al. This is due to the fact that machine learning algorithms can quickly solve inverse problems from the collected data by means of supervised learning, utilizing strong data fitting capabilities. This is also the motivation for us to develop a deep learning method for aerosol concentration inversion under LIDAR remote sensing sparse sampling.

In this work, we present an End-to-end deep network framework, which can first map LIDAR return signals under sparse sampling into a high-dimensional space to realize the high-dimensional feature representation learning of LIDAR return signals; then this feature with high information density can be reconstructed as an accurate aerosol extinction coefficient distribution. Experiments based on Mie scattering LIDAR show that the accuracy of the proposed sparse reconstruction method is similar to that of the reconstruction method with full sampling, which indicates that the proposed method has the potential to improve the efficiency of aerosol LIDAR remote sensing measurement.

Algorithm 1 The Implemented Steps for the Generative Adversarial Network

Input: The training set D, the number of iterations of adversarial training T, the number of training iterations of discriminant network K, and the number of small-batch samples M

Random initialization θ, ϕ;

for $t \leftarrow 1$ to T **do**

  // Training discriminant network $D(x; \phi)$

  for $k \leftarrow 1$ to K **do**

    // Collect small batches of samples

    M samples were collected from the training set D, $\{x^{(m)}\}$, $1 \le m \le M$;

    M samples were collected from the distribution $N(0, I)$, $\{z^{(m)}\}$, $1 \le m \le M$;

    Update ϕ up using a random gradient where the gradient is $\frac{\partial}{\partial \phi}\left[\frac{1}{M}\sum_{m=1}^{M}\left(\log D(x^{(m)}; \phi) + \log\left(1 - D\left(G(x^{(m)}; \theta); \phi\right)\right)\right)\right]$;

  end for

  // Training generative network $G(z; \theta)$

  M samples were collected from the distribution $N(0, I)$, $\{z^{(m)}\}$, $1 \le m \le M$;

  Update ϕ up using a random gradient where the gradient is $\frac{\partial}{\partial \theta}\left[\frac{1}{M}\sum_{m=1}^{M} D(G(z^{(m)}; \theta), \phi)\right]$;

end for

Output: Generative network $G(z; \theta)$

II. PROBLEM FORMULATION

Since the formula of the LIDAR return signals of the Mie scattering lidar is relatively complex, in order to solve the parameters such as the aerosol extinction coefficient, the traditional extinction coefficient inversion algorithm needs to propose some assumptions to simplify the principle formula, which makes the algorithm less accurate. For example, the Collis slope method assumes that the extinction coefficient and backscattering sparsity are constant values at the same height. The Fernald integral method considers both the extinction coefficient and backscattering coefficient contributions of aerosols and atmospheric molecules by assuming the extinction-backscattering ratio of molecules and aerosols. Then, the boundary value of the extinction coefficient of the molecule is obtained from the atmospheric model. Therefore, as long as the boundary value of the aerosol extinction coefficient at the reference distance is obtained on the

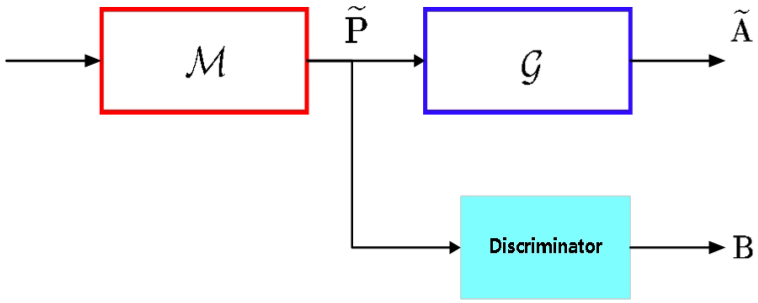

FIGURE 1. The generative adversarial network architecture to generate the extinction coefficient matrix, where the output of the discriminator network is B.

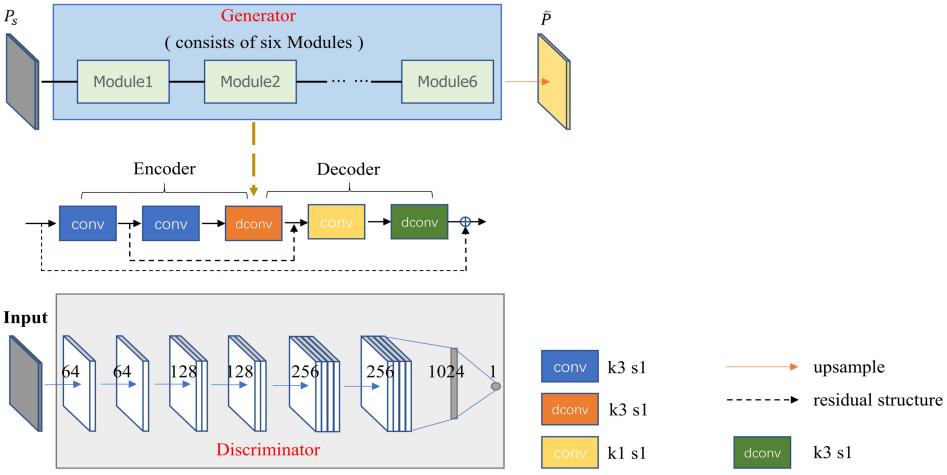

FIGURE 2. The proposed unsupervised generative adversarial networks. k is the size of the convolution kernel and s is the step size.

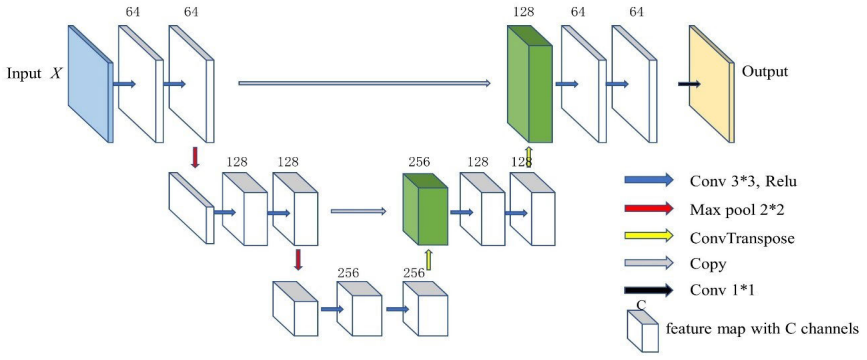

FIGURE 3. The proposed fast reconstruction deep network.

detection path, the extinction coefficient at any distance on the detection path can be defined as Eq.1 and Eq.2, shown at the bottom of the next page.

where $\alpha_a(r)$ denote the aerosol extinction coefficient at distance r, $\alpha_m(r)$ denote the atmospheric molecular extinction coefficient, $\beta_a(r)$ denote the aerosol backscattering coefficient, $\beta_m(r)$ denote the atmospheric molecular backscattering coefficient [12]. P is the return signals received by the LIDAR, r_c denotes the reference distance. For 532nm wavelengths, $S_a = \frac{\alpha_a(r)}{\beta_a(r)} = 50$. The extinction backscattering ratio of atmospheric molecules is given by $S_m = \frac{\alpha_m(r)}{\beta_m(r)} = \frac{8\Pi}{3}$ [13]. However, the application of this method in the real-time inversion of aerosol concentration distribution needs to face two challenges. First of all, the method artificially introduces prior information, so the extinction coefficient obtained is not accurate. Secondly, the time complexity of the method is high, which makes the inversion time too long.

Unlike the representations in above Eqs, if we represent the relationship between return signals and extinction coefficient simply as the mapping $\mathcal{G}$ shown in Eq.3:

$$\mathbf{A} = \mathcal{G}(\mathbf{P}), \quad \mathbf{A} \in \mathbb{R}^{ij}, \ \mathbf{P} \in \mathbb{R}^{kl} \tag{3}$$

where, $\mathbf{A}$ means the discretized distrubution of $\alpha_a(r)$, and $\mathbf{P}$ means the discretized distrubution of $P(r)$; (i, j) and (k, l)

mean sizes of $\mathbf{A}$ and $\mathbf{P}$. Obviously, an end-to-end deep neural network framework can be built to achieve real-time accurate inversion of aerosol extinction coefficients through supervised learning based on the dataset $D = (\mathbf{P}^n, \mathbf{A}^n)_{n=1}^N$.

If we consider improving the reconstruction speed of aerosol concentration through sparse sampling, then Eq.3 can be further expressed as Eq.4:

$$\widetilde{\mathbf{A}} = \mathcal{G}\mathcal{M}(\mathbf{P}_s), \quad \widetilde{\mathbf{A}} \in \mathbb{R}^{ij}, \ \mathbf{P}_s \in \mathbb{R}^{k'l'} \tag{4}$$

where, $\widetilde{\mathbf{A}}$ is the estimate of $\mathbf{A}$, $\mathcal{M}(\mathbf{P}_s) = \widetilde{\mathbf{P}}$, $\widetilde{\mathbf{P}}$ is the estimate of $\mathbf{P}$, the $\mathbf{P}_s$ means the discretized sparse sampling distrubution of $P(r)$, and (k', l') mean sizes of $\mathbf{P}_s$. Clearly, the network $\mathcal{G}$ obtained through supervised learning on dataset D cannot be directly applied to the mapping from $\mathbf{P}_s$ to $\mathbf{A}$, because $\mathbf{P}_s$ and $\mathbf{P}$ has significant differences in feature distribution, that is $p(\mathbf{P}_s) \neq p(\mathbf{P})$. So, a key issue that needs to be addressed is, how to construct a mapping $\mathcal{M}$ in the form of a deep neural network based on the dataset D.

III. MODEL

A feasible solution to the problem of constructing a deep network $\mathcal{M}$ raised in section II is to use transfer learning methods to eliminate the differences between $p(\mathbf{P}_s)$ and $p(\mathbf{P})$. In this work, we attempt to construct a Generative Adversarial Network using unsupervised learning methods, where the generator network can generate echo signal matrix with the same probability distribution as $\mathbf{P}$ based on the sparse sampled return signal matrix $\mathbf{P}_s$. Due to the rich dense sampling return signal matrix $\mathbf{P}$ and extinction coefficient matrix $\mathbf{A}$ obtained from Eq.1 and Eq.2 in the early research on LIDAR, we can conveniently construct the dataset $D = (\mathbf{P}^n, \mathbf{A}^n)_{n=1}^N$. Based on the return singal matrix $\mathbf{P}$ constructed by the generation network $\mathcal{M}$, we can further use supervised learning to construct a deep network $\mathcal{G}$ on the basis of dataset D, and then achieve end-to-end reconstruction from sparse sampling return signal matrix $\mathbf{P}_s$ to extinction coefficient matrix $\mathbf{A}$. The structure of the GAN can be given as Fig.1.

In this paper, deep learning technology is introduced. The proposed network is based on GAN(Generative Adversarial Network), as shown in Fig. 2., using a total of six reconstruction modules, adopting a ''step by step'' strategy to gradually reconstruct the sparse sampling data, and finally obtaining high-quality reconstruction data under the superposition of multiple modules. Here we use pseudocode to show the steps of GAN implementation. The reconstruction structure is modularized, and the balance between data accuracy and reconstruction time can be sought by changing the number of modules. The reconstruction module is an encoder-decoder structure, which mainly consists of two convolution, two deconvolution, residual structure and Skip-connection, and the activation function is Relu(Rectified Linear Unit), which can improve the nonlinear fitting ability of the neural network and thus increase the expression ability of the model. The sparsely sampled data are first encoded by two convolutions, which are operated with 32 convolution kernels of size 3*3 with a step size of one. Then, a deconvolution of 32 convolution kernels with size 3*3 and step size 1 and a deconvolution of 1 convolution kernel with size 3*3 and step size 1 were used for decoding, respectively. Skip-connection is used to combine low-level high-resolution features with high-level semantics to ensure the details of the reconstructed data. Then, the number of feature channels is unified by convolution with convolution kernel size of 1*1 and step size of 1. At the end of the reconstruction module, the residual structure was used to add the input and the learned residual bitwise to prevent the explosion and disappearance of the network gradient. Finally, the upsampling function was used to map the reconstructed data into a high-dimensional space.

The corresponding discriminator contains six convolutional layers with 64, 64, 128, 128, 256 and 256 convolution kernels, respectively. The size of the convolution kernel is 3*3, the step size is 1, and the 'SAME' convolution is used, and the activation function is Relu. This is followed by two fully connected layers with 1024 and 1 neurons, respectively.

An end-to-end deep neural network framework is proposed to achieve real-time accurate inversion of aerosol extinction coefficients under sparse sampling. Specifically, given a training set $D = (x^n, y^n)_{n=1}^N$, where x^n represents the intensity of the LIDAR return signals in the sparse observation area, and y^n represents the high-dimensional extinction coefficient of the observation area. The proposed network first uses the bicubic interpolation method to increase the dimension of x^n to the desired dimension (that is, consistent with y^n), which is still recorded as x^n. Then, through the encoder-decoder structure, the intensity of the LIDAR return signals is reconstructed as the aerosol extinction coefficient. The loss function in this process can be defined as:

$$R(\theta) = \frac{1}{N}\sum_{n=1}^{N} L\left(y^n, f\left(x^n;\theta\right)\right) + \lambda_1 l_1(\theta) + \lambda_2 l_2(\theta) \tag{5}$$

$$\alpha_a(r) = -\frac{S_a}{S_m}\cdot\alpha_m(r) + \frac{P(r)r^2\cdot\exp\left[2\left(\frac{S_a}{S_m}-1\right)\int_r^{r_c}\alpha_m\left(r'\right)dr'\right]}{\frac{P(r_c)r^2}{\alpha_a(r_c)+\frac{S_a}{S_m}\alpha_m(r_c)} + 2\int_r^{r_c} P\left(r'\right)r^2\exp\left[2\left(\frac{S_a}{S_m}-1\right)\int_r^{r_c}\alpha_m\left(r''\right)dr''\right]dr'} \tag{1}$$

$$\alpha_a(r) = -\frac{S_a}{S_m}\cdot\alpha_m(r) + \frac{P(r)r^2\cdot\exp\left[-2\left(\frac{S_a}{S_m}-1\right)\int_{c_c}^{r}\alpha_m(r')dr'\right]}{\frac{P(r_c)r^2}{\alpha_a(r_c)+\frac{S_a}{m}\alpha_m(r_c)} - 2\int_{r_c}^{r} P(r')r^2\exp\left[-2\left(\frac{S_a}{S_m}-1\right)\int_{r_c}^{r}\alpha_m(r'')dr''\right]dr'} \tag{2}$$

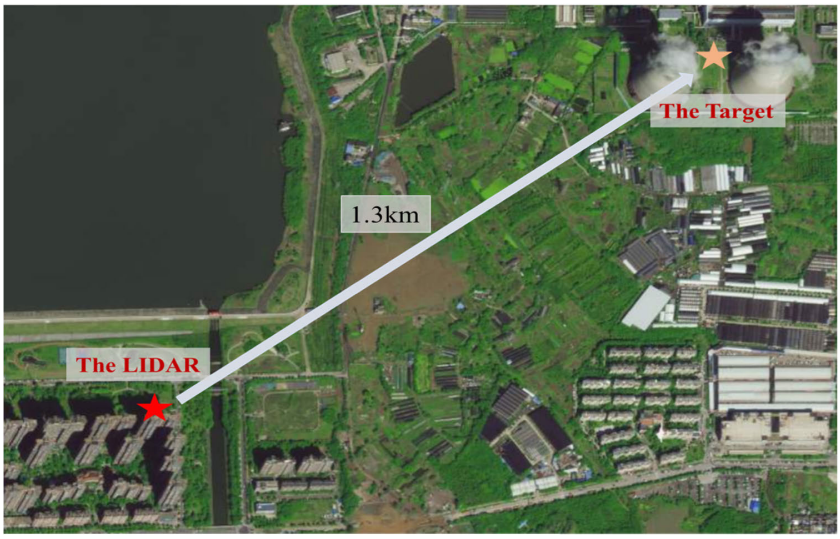

FIGURE 4. Schematic diagram of the measurement point position.

TABLE 1. Performance comparison.

Methods	20211216		20211217		20211218	
	SNR	SSIM	SNR	SSIM	SNR	SSIM
Nearest-neighbor	26.88	0.64	22.29	0.43	25.37	0.57
Bilinear	28.32	0.80	29.42	0.74	27.99	0.68
Bicubic	30.37	0.85	32.81	0.83	31.03	0.79
EDSR	32.52	0.83	32.87	0.84	33.11	0.84
RCAN	33.61	0.85	34.19	0.87	33.91	0.86
Ours	**36.00**	**0.92**	**35.75**	**0.89**	**35.99**	**0.91**

FIGURE 5. The LIDAR.

FIGURE 6. The thermal power plant.

where l_1 and l_2 represent the regularization term of the l_1 norm and the regularization term of the l_2 norm, respectively. Therefore, the optimization goal of the proposed network is:

$$\theta^* = \operatorname{argmin} R(\theta) \tag{6}$$

In order to realize the real-time inversion of the aerosol extinction coefficient, this paper attempts to use the LIDAR return signals under sparse sampling to reduce the sampling time and speed up the inversion of the aerosol extinction coefficient. Due to the sparsely sampled data, in order to increase the spatial resolution of the aerosol extinction coefficient, we use bicubic interpolation to increase the spatial resolution of the input LIDAR return signals to the required size before feeding it into the designed network structure. This method reduces the number of lidar sampling, and then reduces the required inversion time. The adopted network structure is shown in Fig. 3.

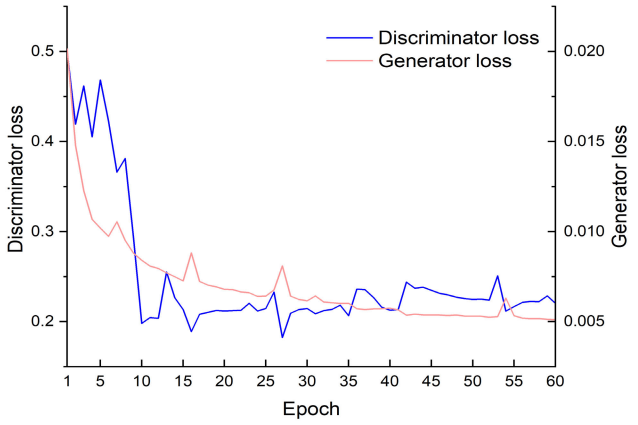

FIGURE 7. The loss change curve of the training phase.

TABLE 2. Comparison of algorithm performance under different sampling rates.

Sampling Rate	1/64	1/16	1/4
SNR	22.29	30.02	36.00
SSIM	0.42	0.76	0.92

The network adopts the classic Encoder-Decoder structure [15], which increases the accuracy of aerosol extinction coefficient by combining high resolution features with low resolution features. This paper adopts the idea of Pre-upsampling, i.e., the resoulution of the input is firstly increased to the target resolution using the bicubic method, and then input into the network to calculate the aerosol extinction coefficient.

The feature extractor we used adopts an alternating structure of two convolutional layers and one pooling layer. Our network can accommodate any size of input images. Here we take an image with a size of $256 \times 256 \times 3$ for example. Assuming that the size of the input images X is $256 \times 256 \times 3$, the sizes of the three-level features from low to high are: $X_1 : 256 \times 256 \times 64$; $X_2 : 128 \times 128 \times 128$; $X_3 : 64 \times 64 \times 256$. The network extracts features layer by layer. X_3 will be the input of the deconvolutional layers, and then the feature fusion module combines the output of the deconvolutional layers with the feature X_2, and then repeat the operation in turn. This kind of skip-connection joins the features of different levels together with complementary information and therefore improves the accuracy.

IV. EXPERIMENTS AND COMPARATIVE ANALYSES

We first briefly describe the relevant experimental Settings and then present the experimental results.

A. EXPERIMENTAL DATASET

The experimental address is located near Silihe Thermal Power Plant, Luyang District, Hefei City (31.90566418°N, 117.23774834°E), as shown in Fig. 4, and the 15th floor of the side household of China Railway International City (Guangyuan) is rented. The LIDAR sends pulse beam to the smoke of the thermal power plant for scanning test, as shown in Fig. 5 and Fig. 6. It is expected to use the smoke aerosol laser backscattering signal to obtain the chimney smoke profile and spatial intensity distribution, and the LIDAR measurement point position is shown in Fig. 4. We first scanned horizontally, then lifted vertically at a fixed angle and then scanned horizontally. The horizontal angle ranged from $-20°$ to $20°$ and the vertical angle ranged from $5°$ to $15°$. We use this dataset to evaluate our proposed network and compare it with existing methods. We set the ratio of the training set, validation set, and testing set as 8:1:1.

B. EXPERIMENTAL ENVIRONMENT

All of the experiments are executed on a computer with NVIDIA GeForce RTX 3090 GPU. The network is implemented by PyTorch. In the training process, we utilize autoencoder to get initial parameters and use a stochastic gradient descent scheme with a batch size of 64 samples, the momentum is 0.9, the weight decay is 0.0005, the initial learning rate is 0.01. The loss change curve of the proposed unsupervised generative adversarial networks are shown in Fig. 7.

C. EVALUATION METRICS

In this paper, structural similarity index (SSIM) and signal-to-noise ratio (SNR) were used to evaluate the performance of the proposed method.

SSIM is a metric to measure the similarity of two structures, which can usually be described as:

$$\begin{aligned}&\mathrm{SSIM}\left(I^{com}, I^{G}\right)\\&= \frac{\left(2\mu_{I^{com}}\mu_{I^{G}} + C_1\right)\left(2\sigma_{I^{com}I^{G}} + C_2\right)}{\left(\mu_{I^{com}}^2 + \mu_{I^{G}}^2 + C_1\right)\left(\sigma_{I^{com}}^2 + \sigma_{I^{G}}^2 + C_2\right)}\end{aligned} \tag{7}$$

where, $\mu_{I^{com}}$ is the average value of I^{com}, μ_{I^G} is the average value of I^G, $\sigma_{I^{com}}^2$ is the variance of I^{com}, $\sigma_{I^G}^2$ is the variance of I^G, and $\sigma_{I^{com}I^G}$ is the covariance of I^{com} and I^G. $C_1 = (k_1 L)^2$ and $C_2 = (k_2 L)^2$ are constants used to maintain stability, L is the dynamic range, $k_1 = 0.01$, $k_2 = 0.03$. The range of SSIM is -1 to 1. When the two structures are the same, the value of SSIM is equal to 1.

PSNR is often used as an evaluation method for signal reconstruction. A higher PSNR indicates that the generated data has a higher quality. It can also be defined by MSE:

$$PSNR(I^{com}, I^{G}) = 10 \cdot \log_{10}\left(\frac{MAX_I^2}{MSE(I^{com}, I^{G})}\right) \tag{8}$$

where, MAX_I represents the maximum possible value of the data.

D. COMPARATIVE EXPERIMENT

In this section, we compare the performance of the proposed network with some existing deep learning-based methods and commonly used interpolation-based methods, including EDSR(enhanced deep super-resolution network) [16],

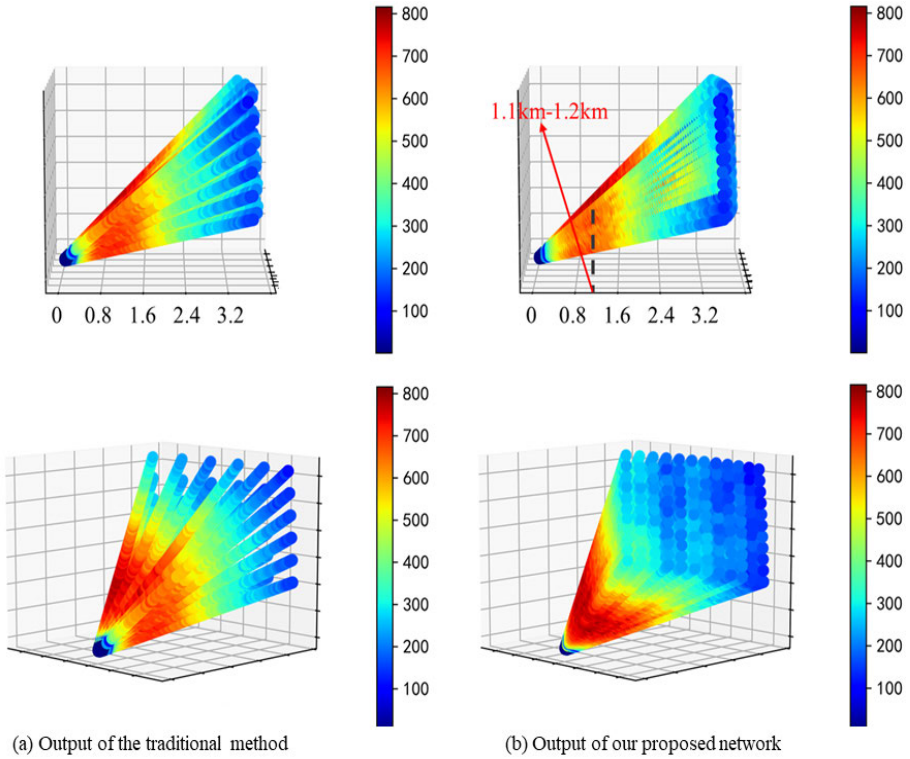

FIGURE 8. Visualization of the spatial distribution of aerosols.

RCAN(residual channel attention networks) [17], nearest-neighbor interpolation, bilinear interpolation and bicubic interpolation. The interpolation-based method means that the sparse aerosol extinction coefficient is first calculated using the traditional algorithm, i.e. Fernald integral method, and then the interpolation method is used to increase its spatial resolution.

We use three days of LIDAR data from December 16, 2021 to December 18, 2021 for our experiments. The experimental results are shown in Table 1. It can be seen that the proposed network outperforms the other methods on all three days of data. The algorithm proposed in this paper firstly uses GAN-based network to gradually reconstruct sparse sampled data to improve the quality of sparse sampled data, and then uses end-to-end fast reconstruction network to invert aerosol extinction coefficient. Therefore, the performance of the algorithm is superior to existing deep learning algorithms. Compare to the interpolation-based algorithm only considering the data relationship between adjacent points to increase the spatial resolution of the aerosol extinction coefficient, the proposed network first maps the sparse LIDAR return signals $\mathbf{P}_s$ into the high-dimensional space, i.e. $\widetilde{\mathbf{P}}$, and then establishes the mapping relationship with the high-resolution aerosol extinction coefficient distribution $\widetilde{\mathbf{A}}$ through the deep neural network, so that the aerosol extinction coefficient can be calculated more accurately. In this paper, we use the method based on deep learning to realize the real-time inversion of aerosol extinction coefficient.

E. ROBUSTNESS EVALUATION

In this section, we test the performance of the proposed network at different sampling rates, that is, how sparse the data can be and how much sampling time can be reduced. We use the LIDAR data on December 16, 2021 for our experiments. The experimental results are shown in Table 2. It can be seen that the proposed network can accurately calculate the aerosol extinction coefficient when the sampling rate is 1/4. When the sampling rate is 1/16, the performance of the algorithm is greatly reduced, but the inversion accuracy is still maintained. However, when the sampling rate is 1/64, the algorithm has been difficult to accurately calculate the aerosol extinction coefficient. It can be concluded that the algorithm can achieve a trade-off between computational accuracy and reconstruction time when only a quarter of the data is sampled, which means that the measurement speed based on our proposed end-to-end method is 4 times that of the traditional measurement method in theory.

F. VISUALIZATION RESULT

Taking the sampling rate 1/4 of the original measurement data as an example, we also give some visualization results in Fig. 8, where (a) represents the aerosol extinction coefficient map calculated directly from the sparsely sampled data using the traditional algorithm, while (b) represents the output of the proposed network. Based on the distance between the edge of the target region and the LIDAR (measured by the map Fig. 4), we can effectively evaluate the performance

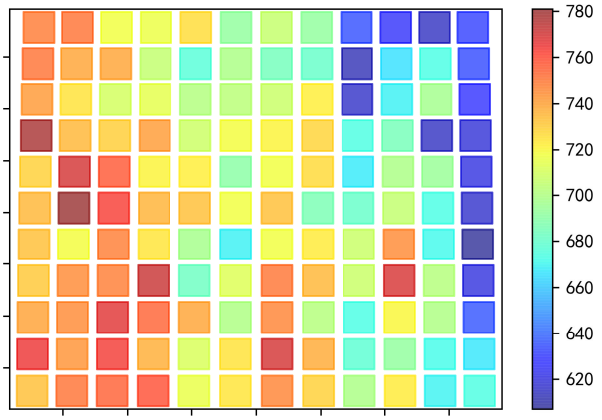

(a) Sparse sampling result.

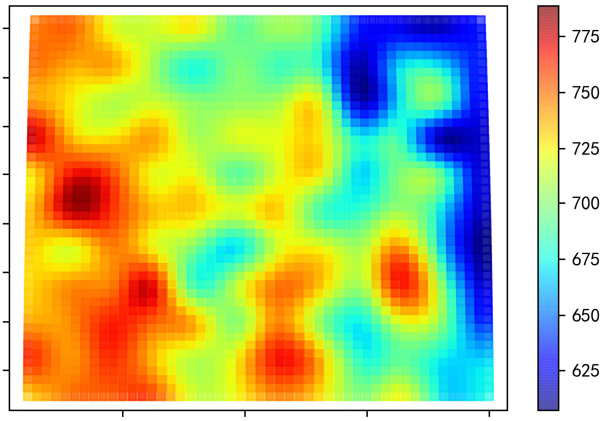

(b) The output of the proposed method.

FIGURE 9. Visualization of vertical slices of aerosols.

of the proposed method. Fig. 4 shows that the distance between LIDAR and the central point of the target region is 1.3km, which is close to the center of the target area shown in Fig. 8 (b) (the distance from center position to LIDAR is 1.1km - 1.2km, the deviation is less than 20). This result proves that the proposed neural network reconstruction method has advantages in Sparse Inversion of Aerosol Concentration Distribution based on LIDAR.

In addition, we visualize part of the results for different slices of one scan cycle as shown in Fig. 9. It can be seen that the proposed algorithm can use sparse sampling data to achieve more detailed and accurate aerosol concentration inversion.

V. CONCLUSION

In this work, we propose an End-to-end deep sparse reconstruction framework for aerosol LIDAR remote sensing fast measurement. This framework first map LIDAR return signals under sparse sampling into a high-dimensional space to realize the high-dimensional feature representation learning of LIDAR return signals, and then this feature with high information density can be reconstructed as an accurate aerosol extinction coefficient distribution. In this way, we can greatly reduce the number of LIDAR samples and thus reduce the measurement time. To verify the effectiveness of the End-to-end method, the experiments based on Mie scattering LIDAR was carried out. The results show that the accuracy of the proposed sparse reconstruction method is similar to that of the reconstruction method with full sampling, which indicates that the proposed method has the potential to improve the efficiency of aerosol LIDAR remote sensing measurement. In the future work, we will further improve the mechanical structure of LIDAR to adapt to the sparse reconstruction framework, and conduct on-line rapid remote sensing tests on the improved fast LIDAR.

ACKNOWLEDGMENT

The authors would like to thank the Hefei Advanced Computing Center for the help with numerical calculations.

REFERENCES

[1] D. Y. H. Pui, S.-C. Chen, and Z. Zuo, "$PM_{2.5}$ in China: Measurements, sources, visibility and health effects, and mitigation," *Particuology*, vol. 13, pp. 1–26, Apr. 2014.
[2] C. K. Chan and X. Yao, "Air pollution in mega cities in China," *Atmos. Environ.*, vol. 42, no. 1, pp. 1–42, Jan. 2008.
[3] H. Kan, R. Chen, and S. Tong, "Ambient air pollution, climate change, and population health in China," *Environ. Int.*, vol. 42, pp. 10–19, Jul. 2012.
[4] H. Jian-Ping, H. Zhong-Wei, B. Jian-Rong, Z. Wu, and Z. Lei, "Micropulse LiDAR measurements of aerosol vertical structure over the loess Plateau," *Atmos. Ocean. Sci. Lett.*, vol. 1, no. 1, pp. 8–11, Jan. 2008.
[5] I. Veselovskii, A. Kolgotin, V. Griaznov, D. Müller, K. Franke, and D. N. Whiteman, "Inversion of multiwavelength Raman LiDAR data for retrieval of bimodal aerosol size distribution," *Appl. Opt.*, vol. 43, no. 5, pp. 1180–1195, 2004.
[6] P. Chazette, J. Pelon, C. Moulin, F. Dulac, I. Carrasco, W. Guelle, P. Bousquet, and P.-H. Flamant, "LiDAR and satellite retrieval of dust aerosols over the Azores during SOFIA/ASTEX," *Atmos. Environ.*, vol. 35, no. 25, pp. 4297–4304, Sep. 2001.
[7] R. T. H. Collis and E. E. Uthe, "Mie scattering techniques for air pollution measurement with lasers," *Opto-Electron.*, vol. 4, no. 2, pp. 87–99, May 1972.
[8] G. Fiocco and L. D. Smullin, "Detection of scattering layers in the upper atmosphere (60–140 km) by optical radar," *Nature*, vol. 199, no. 4900, pp. 1275–1276, Sep. 1963.
[9] C.-Y. She, "Spectral structure of laser light scattering revisited: Bandwidths of nonresonant scattering LiDARS," *Appl. Opt.*, vol. 40, no. 27, pp. 4875–4884, 2001.
[10] R. T. H. Collis, "LiDAR: A new atmospheric probe," *Quart. J. Roy. Meteorological Soc.*, vol. 92, no. 392, pp. 220–230, Apr. 1966.
[11] J. D. Klett, "Stable analytical inversion solution for processing LiDAR returns," *Appl. Opt.*, vol. 20, no. 2, pp. 211–220, 1981.
[12] F. G. Fernald, "Analysis of atmospheric LiDAR observations: Some comments," *Appl. Opt.*, vol. 23, no. 5, pp. 652–653, 1984.
[13] Y. Sasano, "Tropospheric aerosol extinction coefficient profiles derived from scanning LiDAR measurements over Tsukuba, Japan, from 1990 to 1993," *Appl. Opt.*, vol. 35, no. 24, pp. 4941–4952, 1996.
[14] G. A. Kaloshin, "Modeling the aerosol extinction in marine and coastal areas," *IEEE Geosci. Remote Sens. Lett.*, vol. 18, no. 3, pp. 376–380, Mar. 2021.
[15] O. Ronneberger, P. Fischer, and T. Brox, "U-Net: Convolutional networks for biomedical image segmentation," in *Proc. Int. Conf. Med. Image Comput. Comput.-Assist. Intervent.* Cham, Switzerland: Springer, 2015, pp. 234–241.
[16] B. Lim, S. Son, H. Kim, S. Nah, and K. M. Lee, "Enhanced deep residual networks for single image super-resolution," in *Proc. IEEE Conf. Comput. Vis. Pattern Recognit. Workshops (CVPRW)*, Jul. 2017, pp. 1132–1140.
[17] Y. Zhang, K. Li, K. Li, L. Wang, B. Zhong, and Y. Fu, "Image super-resolution using very deep residual channel attention networks," in *Computer Vision—ECCV*, V. Ferrari, M. Hebert, C. Sminchisescu, and Y. Weiss, Eds. Cham, Switzerland: Springer, 2018, pp. 294–310.

WEIYI WANG is currently pursuing the Ph.D. degree with the Hefei Institutes of Physical Science, Chinese Academy of Sciences, and the University of Science and Technology of China. Her research interest includes laser remote sensing imaging technology.

DONGSHENG YU is currently an Associate Research Fellow with the Hefei Institutes of Physical Science, Chinese Academy of Sciences. His research interest includes the development and application of laser remote sensing equipment and technology.

HAIBO YU received the master's degree from Jiangnan University, Wuxi, China, in 2022. He is currently pursuing the Ph.D. degree with the University of Science and Technology of China, Hefei, China. His research interests include image forensics, semantic segmentation, and artificial intelligence.

MINGHAN YANG received the Ph.D. degree from the University of Chinese Academy of Sciences, Hefei, China, in 2016. He is currently an Associate Professor with the Nuclear Emergency and Public Safety Laboratory, Institute of Nuclear Energy Safety Technology, Hefei Institute of Physical Sciences, Chinese Academy of Sciences, Hefei. His research interests include imaging technology and system simulation.

CHIDONG XU is currently a Research Fellow with the Hefei Institutes of Physical Science, Chinese Academy of Sciences. He also serves as the Director of the Optoelectronic Detection Technology Century, Anhui Institute of Optics and Fine Mechanics. He has led and participated in various national scientific research projects, including public welfare industry (meteorology) research projects, sub-projects of the 863 Program, key projects of the Basic Research Special Program of the Ministry of Science and Technology, and pre-research projects in aerospace. His research interest includes the development and application of optoelectronic technology and instruments.

XIAODONG FANG is currently a Research Fellow with the Anhui Institute of Optics and Fine Mechanics, Chinese Academy of Sciences. He is a Professor with the Shenzhen University of Technology. He has led national science and technology major projects, national major scientific research instrument development projects, national natural science foundation projects, and equipment development projects of the Chinese Academy of Sciences. His research interest includes the technology and application research of quasi-pulsed laser.